nature nanotechnology

ARTICLES

PUBLISHED ONLINE: 25 AUGUST 2013 | DOI: 10.1038/NNANO.2013.160

Hierarchical patterns of three-dimensional block-copolymer films formed by electrohydrodynamic jet printing and self-assembly

M. Serdar Onses[1†], Chiho Song[1,5†], Lance Williamson[3,4], Erick Sutanto[2], Placid M. Ferreira[2], Andrew G. Alleyne[2], Paul F. Nealey[3,4], Heejoon Ahn[1,5]* and John A. Rogers[1,2]*

Self-assembly of block-copolymers provides a route to the fabrication of small (size, <50 nm) and dense (pitch, <100 nm) features with an accuracy that approaches even the demanding specifications for nanomanufacturing set by the semiconductor industry. A key requirement for practical applications, however, is a rapid, high-resolution method for patterning block-copolymers with different molecular weights and compositions across a wafer surface, with complex geometries and diverse feature sizes. Here we demonstrate that an ultrahigh-resolution jet printing technique that exploits electrohydrodynamic effects can pattern large areas with block-copolymers based on poly(styrene-block-methyl methacrylate) with various molecular weights and compositions. The printed geometries have diameters and linewidths in the sub-500 nm range, line edge roughness as small as ∼45 nm, and thickness uniformity and repeatability that can approach molecular length scales (∼2 nm). Upon thermal annealing on bare, or chemically or topographically structured substrates, such printed patterns yield nanodomains of block-copolymers with well-defined sizes, periodicities and morphologies, in overall layouts that span dimensions from the scale of nanometres (with sizes continuously tunable between 13 nm and 20 nm) to centimetres. As well as its engineering relevance, this methodology enables systematic studies of unusual behaviours of block-copolymers in geometrically confined films.

Self-assembly in block-copolymers (BCPs) holds great promise for applications in nanolithography[1] and the assembly of nanomaterials[2], with demonstrated capabilities in the fabrication of nanoscale devices[3,4]. When confined in thin films, phase-separated BCPs[5] can serve as resist layers with feature sizes and densities that are difficult or impossible to achieve with conventional optical lithography systems. In a scheme known as BCP lithography[6,7], a spin-cast film of BCP self-assembles into nanoscale structures. Selective etching removes one of the blocks, so that the remaining block can act as a conventional resist for patterning an underlying substrate by liftoff or etching. Three main challenges prevent the generalized application of standard BCP lithographic methods that use spin-cast films. First, self-assembly yields randomly oriented nanoscale domains with poor long-range order. Second, spin-casting produces uniform films, without control over the location, size or geometry of the patterned areas. Third, the molecular weight (MW) and composition of the BCP fix the size, periodicity and morphology of the nanoscale domains across the film. Techniques for directed self-assembly (DSA) based on chemically[1,8,9] and topographically[10–13] patterned substrates address the first two limitations. One approach to overcoming the third makes use of the DSA of BCP–homopolymer blends on chemically patterned substrates to access device oriented structures and periodicities that are different from the bulk[14,15]. Sequential solvent annealing together with selective area crosslinking can also locally vary the morphology, size and periodicity of the nanoscale domains[16,17]. However, these procedures allow only modest adjustment of these characteristic dimensions, and do not provide independent control over them. In an alternative strategy, sequential nanoimprinting with two templates prepared using DSA of BCPs with different domain periodicities has been used to create a single master for patterning bits and servo control regions for magnetic storage media[18]. Practical difficulties arise, however, from the need for multiple nanoimprinting steps with overlay registration, as well as intimate, yet non-destructive, physical contact over large sample areas. In fact, such difficulties motivate the development of device and system layouts that can be implemented with only a single characteristic period across the entire area of the substrate. Eliminating such constraints could be valuable in many different application contexts.

Electrohydrodynamic jet printing of BCP films

In the following, we demonstrate the use of an advanced form of electrohydrodynamic jet printing[19] to define arbitrary patterns of BCP films with independent control of the size, periodicity and morphology of the resulting nanoscale domains, in a manner that does not involve physical contact with the substrate. Here, applied electric fields drive flow of 'inks' from nozzles, to achieve droplet sizes as small as ∼100 nm (refs 20,21). Multiple nozzles[22] allow rapid and purely additive patterning of multiple ink formulations, with accurate registration. Inks based on poly(styrene-block-methyl methacrylate) (PS-b-PMMA) can be routinely printed as

[1]Department of Materials Science and Engineering, Beckman Institute, and Frederick Seitz Materials Research Laboratory, University of Illinois at Urbana-Champaign, Urbana, Illinois 61801, USA, [2]Department of Mechanical Science and Engineering, University of Illinois at Urbana-Champaign, Urbana, Illinois 61801, USA, [3]Institute for Molecular Engineering, The University of Chicago, Chicago, Illinois 60637, USA, [4]Materials Science Division, Argonne National Laboratory, 9700 South Cass Avenue, Argonne, Illinois 60439, USA, [5]Department of Organic and Nano Engineering and Institute of Nano Science and Technology, Hanyang University, 17 Haengdang-Dong, Seongdong-Gu, Seoul 133-791, Korea, †These authors contributed equally to this work.
*e-mail: jrogers@illinois.edu; ahn@hanyang.ac.kr

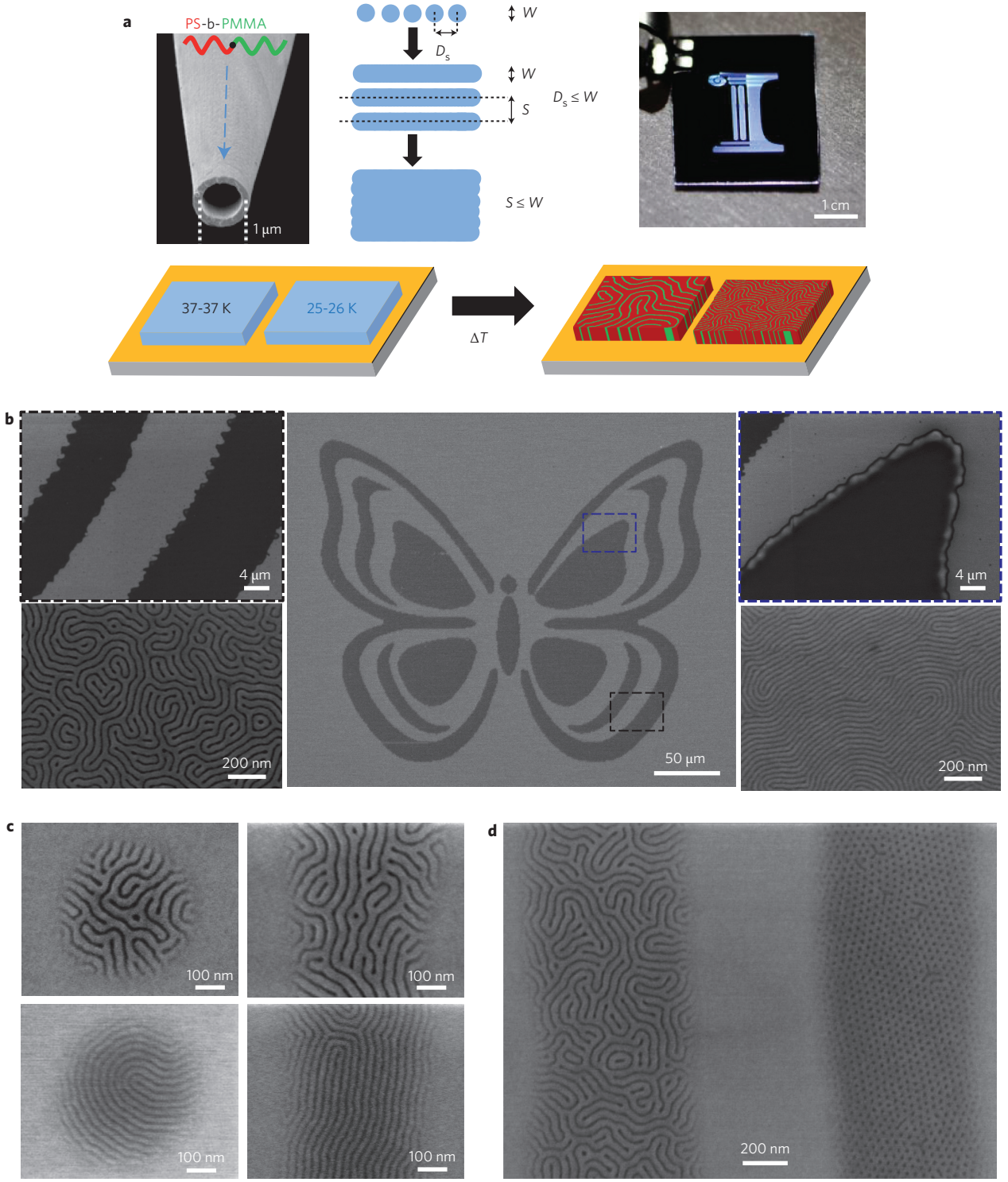

Figure 1 | Electrohydrodynamic jet printing of BCP films. a, Schematic illustration of the process for high-resolution jet printing of PS-b-PMMA through fine nozzles by the action of electrohydrodynamic forces. The left frame shows an SEM image of the end tip of a glass capillary nozzle coated with Au/Pd. Applying a voltage between this nozzle and a grounded substrate induces controlled printing of droplets or linear streams of BCP dissolved in an organic solvent. A computer-controlled stage moves the substrate relative to the nozzle, to allow automated printing of arbitrary patterns of BCPs. As shown schematically at the top, operation in a raster scanning mode allows patterns of droplets (W, diameter; D_s, droplet spacing) to define lines (W, width; S, line spacing), and lines to define areas. Thermal annealing (220 °C for 5 min) results in the self-assembly of BCPs into nanostructures on a neutral substrate. The image at top right provides an example of a large-area pattern formed using 2% 37-37 K PS-b-PMMA and a nozzle with 10 μm internal diameter. **b**, SEM images of a complex pattern printed with two PS-b-PMMAs with different MWs (0.1% ink and a nozzle with 1 μm internal diameter). The left and right images present high-magnification views of regions printed with 37-37 K ($L_0 = 41$ nm, black dashed box) and 25-26 K ($L_0 = 27$ nm, blue dashed box) PS-b-PMMA, respectively. **c**, Individual dots (left) and lines (right) printed with 37-37 K (top) and 25-26 K (bottom) PS-b-PMMA (0.1% ink and a nozzle with 500 nm internal diameter). **d**, SEM image showing self-assembled nanoscale structures with two different morphologies (lamellae forming 37-37 K, left; cylinder forming 46-21 K, right) printed as lines.

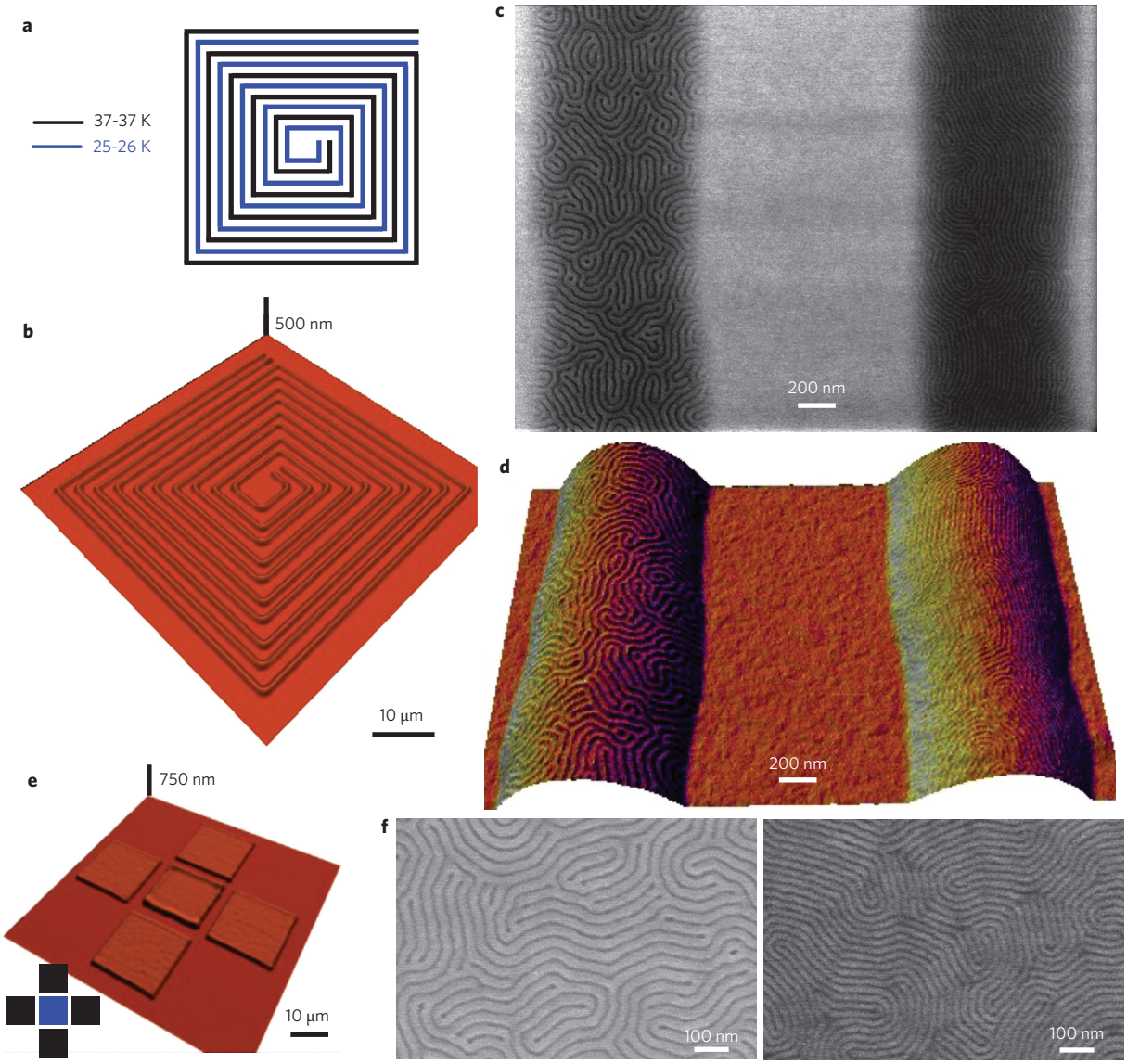

Figure 2 | High-resolution registration in printing of BCPs with different MWs. a, Schematic illustration of a concentric spiral pattern consisting of PS-b-PMMA with MWs of 37-37 K (black) and 25-26 K (blue). **b**, AFM image of the printed pattern. Line widths and spacings are ~800 nm and ~1 μm, respectively. **c**,**d**, High-magnification SEM and AFM images of representative regions of this spiral pattern, showing self-assembled nanoscale structures with different periodicities (41 nm for 37-37 K, left; 27 nm for 25-26 K, right). The AFM includes information from both the amplitude (height) and phase (tip–sample interaction) to illustrate both the topography and the chemical species. The heights of the printed lines at the centre are ~40 nm. **e**, AFM image of a printed pattern of five squares (sides, 20 μm), with edge-to-edge separations of nearest neighbours of 3 μm. The centre and outer squares consist of 25-26 K and 37-37 K PS-b-PMMA, respectively. **f**, High-magnification SEM images of regions of squares printed with 37-37 K (left) and 25-26 K (right). All examples used a neutral substrate, 0.1% ink, a nozzle with 1 μm internal diameter, and thermal annealing after printing.

dots and lines with sub-500 nm dimensions, excellent uniformity and repeatability in thickness (roughness, <2 nm) and user-defined layouts that span length scales from the sub-micrometre to centimetre regimes. These procedures define the location, size and geometry of patterns of BCP films, in a hierarchical lithography process that naturally capitalizes on nanoscale features that form by self-assembly. Precise control over the architecture and registration of the nanoscale domains of BCPs in each printed region can be achieved by printing onto chemically and topographically templated substrates by means of DSA processes.

Figure 1 presents examples that demonstrate the versatility of these processes in terms of printed feature size, geometry and area coverage. The inks consist of dilute (for example, 0.1%) solutions of PS-b-PMMA with different MWs in 1,2,4-trichlorobenzene. Applying a voltage between a grounded substrate and a metal coating on a glass capillary loaded with ink results in the flow of BCPs through a fine nozzle aperture at the tapered tip (for example, 1 μm internal diameter, Fig. 1a inset). A computerized system of translation stages moves the substrate relative to the nozzle and controls the voltage for printing lines or dots in a raster scanning mode. This procedure yields continuous BCP films with programmed micro/nanoscale geometries over macroscopic areas (Fig. 1a) in an automated fashion, eliminating the need for masks and enabling efficient use of the BCP materials. Patterning of multiple BCP inks into complex layouts is also readily achievable, as shown in Fig. 1b. Here, the substrate is a silicon wafer functionalized with a random copolymer mat to provide a surface that is non-preferential (that is, neutral) in wetting towards the PS and PMMA blocks[23]. Thermal annealing induces phase separation of the BCPs into domains oriented

perpendicular to the substrate surface with periodicities determined by the MW. The scanning electron microscope (SEM) images in the left and right columns of Fig. 1b show periodicities (L_0) of 41 nm (body and outer wing; 37-37 K PS-b-PMMA) and 27 nm (inner wing; 25-26 K PS-b-PMMA), respectively. The results in Fig. 1c demonstrate access to sub-500 nm dimensions in isolated dots and lines. Printing BCPs with different volume fractions allows the generation of a variety of nanoscale morphologies (Fig. 1d: lamellar and cylindrical) on the same substrate. The composition[24] of the neutral substrate is critical to achieving the perpendicular orientation of the domains with respect to the substrate for both morphologies.

The accurate registration of patterns formed with different BCP inks is a critical capability. Figure 2 presents two examples achievable with existing set-ups. The first (Fig. 2a) consists of concentric square spiral shapes composed of BCPs with two different MWs, where adjacent lines have separations of ~1 μm. The atomic force microscope (AFM) image in Fig. 2b shows successful printing of the designed pattern. The SEM and AFM images in Fig. 2c,d provide additional detail. A second example consists of square patterns (20×20 μm^2) of BCPs with different MWs separated by 3 μm, shown in the SEM and AFM images of Fig. 2e,f. The results of Fig. 2b, in particular, demonstrate the ability to achieve accurate and uniform registration at the sub-micrometre level, over large areas. Enhanced operation in this regime, and beyond, can be facilitated by replacing the diffraction-limited optical techniques used in the current system with the type of Moiré methods that are successfully applied in conventional and nanoimprint lithography machines.

Programmed printing with multiple passes allows for precise control not only over the lateral dimensions and registration of the printed patterns, but also of their thicknesses. Thickness plays a critical role in the orientation of domains on the chemically homogeneous surfaces that result from BCP self-assembly. In particular, the ratio of thickness to L_0 is a critical parameter, typically selected to be some multiple of 0.5 (ref. 7). A first essential capability is the repeatable control of thickness, in a way that does not depend strongly on characteristic lateral feature sizes. Figure 3a shows examples of printed squares with various dimensions (side dimensions of 15, 10 and 5 μm, corresponding to areas more than 100 times smaller than those that would be possible with conventional ink-jet techniques[25]). The uniformity (<2 nm) and repeatability (<2 nm) in thickness, both measured after annealing, can be remarkably good for films with thicknesses in the range studied here. In particular, the averages and standard deviations in thickness for the three cases shown in Fig. 3a are 26.2 nm, 26.9 nm, 26.1 nm and 1.2 nm, 1.5 nm, 1.6 nm, respectively. To demonstrate capabilities in thickness control over a range relevant for BCP lithography, we printed an array of 25-μm-wide squares with thicknesses between 20 nm and 120 nm. Figure 3b presents an optical micrograph in which interference colours arise from different thicknesses. Systematic experiments of this type can be used to establish calibration curves (Fig. 3c) that are conceptually similar to the spin speed/thickness curves used in spin-casting. A wide range of thicknesses can be accessed through control of other parameters such as the weight percent of the ink, printing speed (Supplementary Fig. S1), applied voltage and standoff height. For a given ink formulation and set of printing conditions, the most straightforward means to adjust the thickness is through the spacing between adjacent printed lines. Lateral flow during annealing leads to uniform thicknesses that depend linearly on the inverse of the spacing.

Together with registration control, this ability to print well-defined amounts of BCPs provides an opportunity to mix two (or more) BCPs with different MWs, at specific relative concentrations, on a substrate surface. This capability enables continuous tuning of

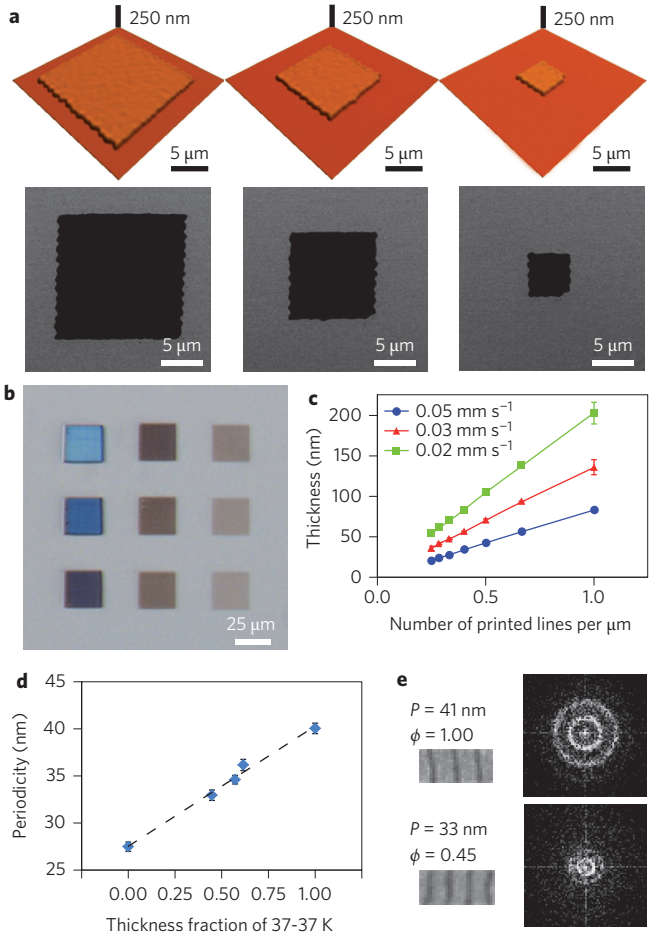

Figure 3 | Precise control over the thicknesses and relative amounts of printed BCPs, with an example of continuous tuning of the periodicities of nanoscale domains. a, AFM (top) and SEM (bottom) images of square films (15, 10 and 5 μm wide) printed using 37-37 K PS-b-PMMA and after thermal annealing. **b**, Optical microscope image of a 3 × 3 array of 25-μm-wide squares with thicknesses ranging from ~20 nm to 120 nm. The examples in all cases were printed using 0.1% ink and a nozzle with 1 μm internal diameter. **c**, Thickness of printed films as a function of number of printed lines per micrometre (inverse of the spacing between consecutive lines). Thicknesses correspond to averages across 50-μm-wide square films printed using a nozzle with 5 μm internal diameter. Error bars indicate variation in the thickness of films across individual squares. **d**, Periodicity P of BCP domains as a function of thickness fraction ϕ of the 37-37 K PS-b-PMMA in a binary mixture with 25-26 K PS-b-PMMA. The mixtures were obtained by sequentially printing 20-μm-wide square films on top of each other. The 37-37 K BCP was printed first. Annealing at 220 °C for 5 min followed printing of both BCPs. Periodicities were calculated through the use of an image analysis algorithm. Error bars indicate standard deviation in the average periodicities measured at different locations. **e**, Representative SEM images and Fourier transforms for two examples. The substrate is neutral wetting for all cases presented above.

the periodicities of the nanoscale domains, defined at the printing step. Figure 3d,e illustrates an example in which printing forms squares of 37-37 K and 25-26 K PS-b-PMMA directly on top of one another. The intimate mixing that occurs during printing and subsequent thermal annealing leads to nanoscale domains with periodicities that lie between the natural values set by the MWs of the BCP (Supplementary Fig. S2 shows an example of a pair of crossed lines). For squares of the same size, the relative ratio of the two copolymers is simply determined by the thickness of each printed film. The periodicity of nanoscale domains in the mixtures

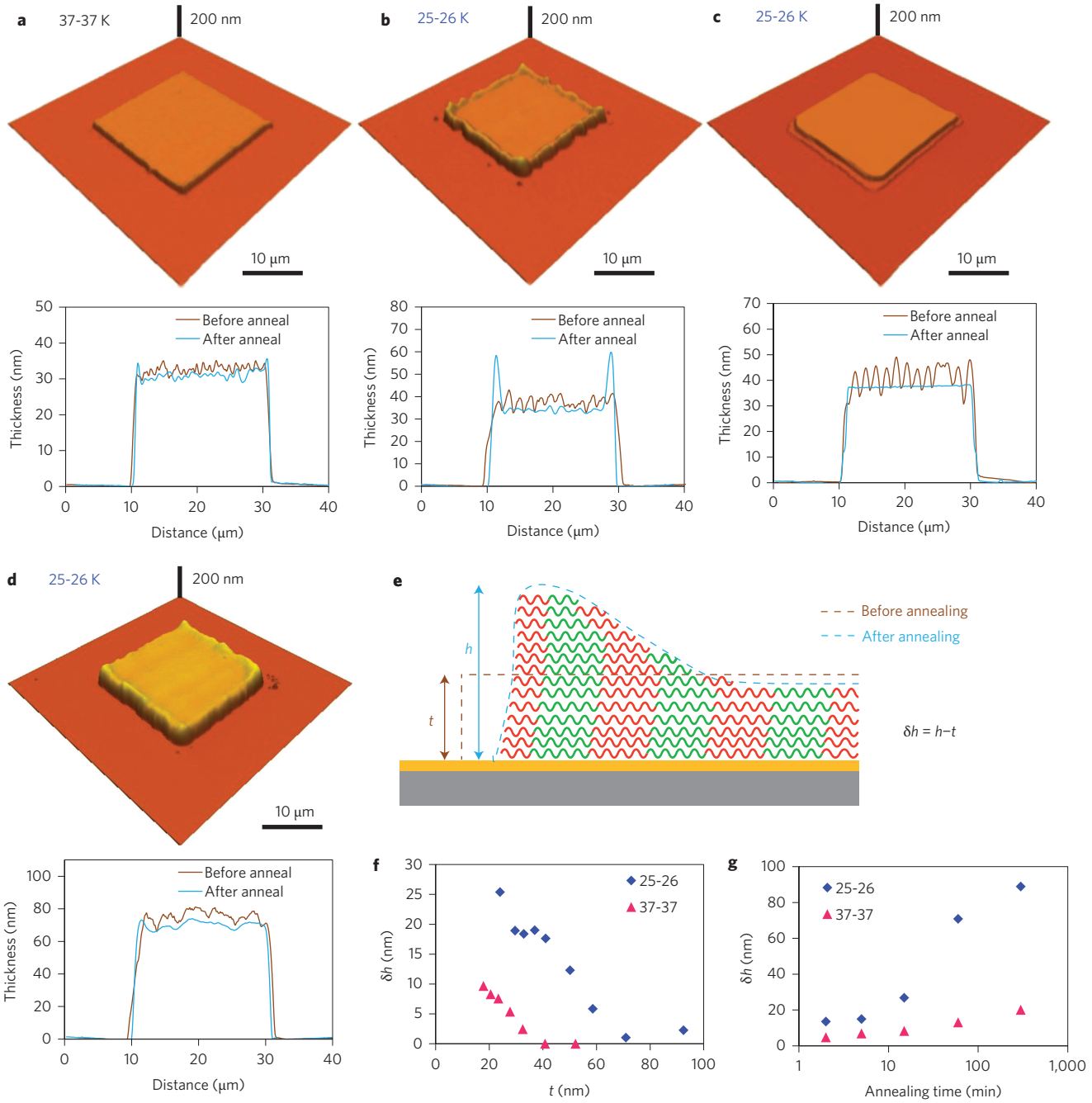

Figure 4 | Analysis of wetting behaviour in BCPs printed onto neutral and preferential wetting substrates. a–d, AFM images (top, after annealing) and cross-sectional height profiles (bottom) of printed squares of PS-b-PMMA. The results illustrate the effects of MW, substrate wetting properties, average thickness and annealing on thickness uniformity. The PMMA block preferentially wets the substrate in **c**, and the substrate is neutral in **a**,**b**,**d**. **e**, Schematic illustration of a printed BCP film near an edge of a square, before and after thermal annealing, for the case of a neutral substrate. The average thickness of printed BCP films before annealing is *t*, and the maximum thickness at the edge of the film after annealing is *h*. The size of the polymer chains is not drawn to scale. **f**,**g**, Increase in film height at the edge (δh) as a function of thickness *t* of the film and annealing time at a temperature of 220 °C.

shows a simple linear dependence on the fraction of an individual BCP present on the surface (Fig. 3d). This dependence agrees well with the previously reported scaling relationship[26], which is approximately linear for BCP blends of similar MWs mixed in solution. This approach to tuning the periodicity has significant practical value because it enables a simple printer system, capable of patterning only two inks, to access a continuously adjustable range of nanoscale feature sizes. Selection of the BCP inks for mixing should account for the miscibility range[27,28] for disparate-molecular-weight BCPs. Concepts of mixing can also be applied to BCPs with different volume fractions or corresponding homopolymers to generate a range of different morphologies on a single substrate.

Wetting behaviour of printed BCP films

The processes of film formation and self-assembly depend strongly on wetting and flow behaviour during annealing. Effects related to MW, substrate functionality and thickness emerge from systematic studies of height profiles of printed patterns of PS-b-PMMA evaluated immediately after printing and subsequent annealing at 220 °C for 5 min. A series of 20-μm-wide square

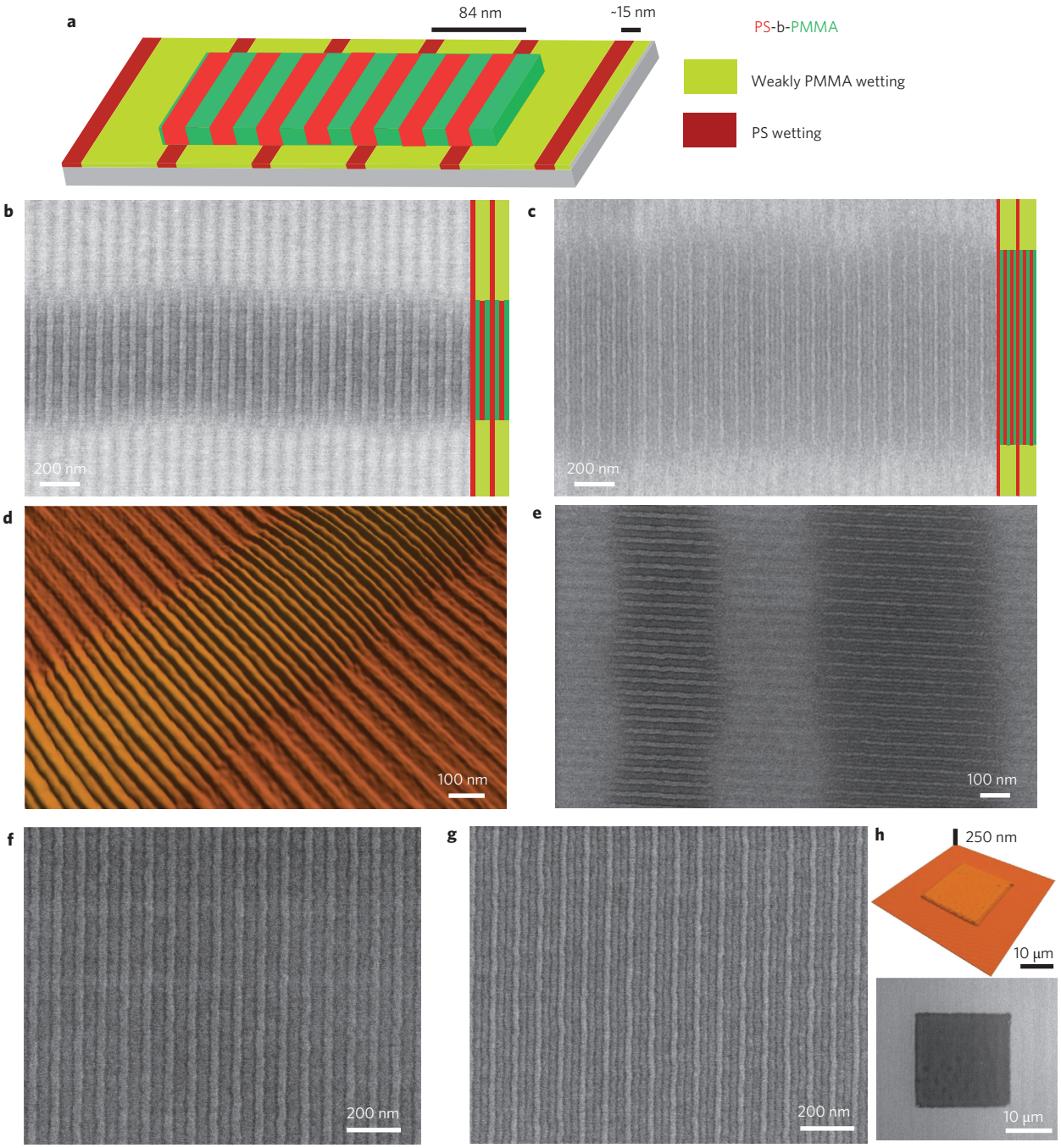

Figure 5 | Directed self-assembly of BCPs printed onto chemically patterned substrates. a, Schematic illustration of the process. **b**,**c**, SEM images of lines of PS-b-PMMA printed onto lithographically defined stripes of PS (~15 nm wide, with 84 nm periodicity). Films made from BCPs with MWs of 37-37 K (**b**) and 25-26 K (**c**) are shown. The results indicate defect-free assembly to produce structures that have twice (**b**) and three times (**c**) the density of the underlying pattern. The rightmost regions of the SEM images are colourized in a way that clarifies the assembly process. **d**, High-resolution AFM image of 37-37 K PS-b-PMMA. **e**, SEM image showing the DSA of BCPs with both MWs, printed as lines with domain sizes of ~20 nm (37-37 K, left) and ~13 nm (25-26 K, right) and separated by ~400 nm, on the same chemical patterned substrate. **f**,**g**, High-magnification SEM images of representative regions of printed squares (20 μm wide, ~20 nm thick) for MWs of 37-37 K (**f**) and 25-26 K (**g**). **h**, AFM (top) and SEM (bottom) images of a square film printed with 25-26 K PS-b-PMMA after thermal annealing at 220 °C for 5 min.

films of varying thicknesses printed using 37-37 K and 25-26 K PS-b-PMMA on neutral (random copolymer mat) and preferential (native oxide terminated silicon) wetting substrates served as the basis of our investigations. Figure 4a–d shows AFM images and cross-sectional height profiles for several examples. Annealing a ~30-nm-thick film of 37-37 K PS-b-PMMA on a neutral substrate leads to a slight decrease in roughness without a significant change in the height profile (Fig. 4a). In contrast, otherwise similar experiments with 25-26 K PS-b-PMMA (Fig. 4b) indicate that material near the edges retracts to form a local region with thickness that is ~30 nm larger than the rest of the film. In addition to this dependence on MW, the wetting properties of the substrate are also important. For example, a printed film of 25-26 K PS-b-PMMA on a preferential wetting substrate (Fig. 4c) has narrow perimeter regions with thicknesses of one layer ($0.5L_0$) and a large central region with a thickness of exactly L_0. The

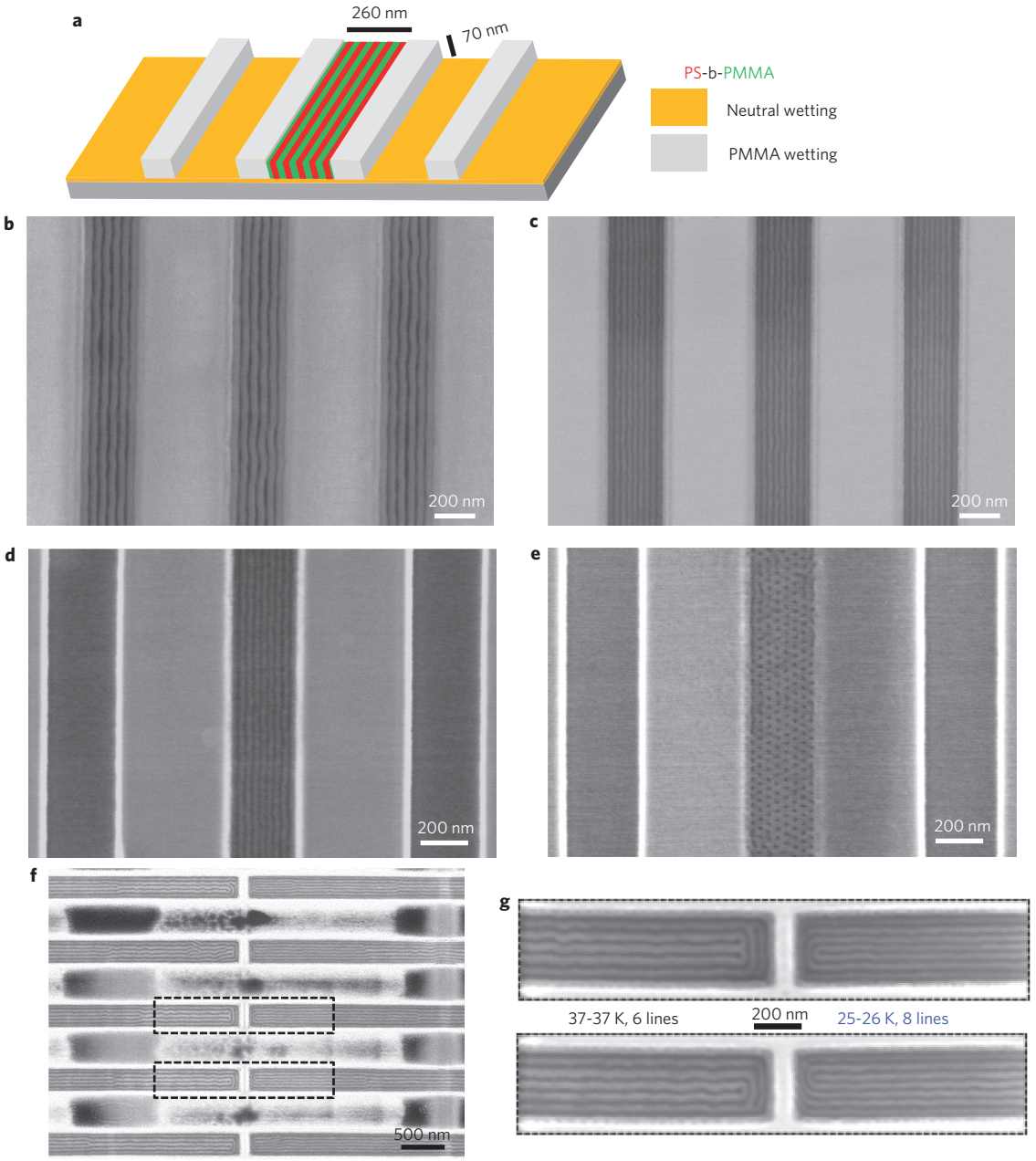

Figure 6 | Directed self-assembly of BCPs printed onto topographically patterned substrates. a, Schematic illustration of the process. **b**,**c**, Representative SEM images showing directed assembly of printed PS-b-PMMA BCPs within trenches (depth ~70 nm, width ~260 nm) defined on a neutral substrate by features of hydrogen silsesquioxane patterned by electron-beam lithography. The examples include BCPs with MWs of 37-37 K (**b**) and 25-26 K (**c**). **d**,**e**, SEM images of BCP lines printed in the direction parallel to the long axis of the trench for 25-26 K (lamellae; **d**) and 46-21 K (cylinder; **e**) PS-b-PMMA. Only one (central) out of three trenches is filled with BCPs. **f**, SEM image showing the directed assembly of BCPs with MWs of 37-37 K (left) and 25-26 K (right) in adjacent trenches. The dark structures on top of the hydrogen silsesquioxane correspond to residual BCP. **g**, High-magnification SEM image of the printed BCP films shown in **f**. Annealing was performed at 250 °C for 5 min in a glove box filled with nitrogen.

perfect flatness of the surface results from a match between the thickness of the printed film and L_0, which corresponds to complete layers of the PMMA and PS blocks at the substrate and air interface, respectively. If the thickness is incommensurate with L_0, then islands/holes (Supplementary Fig. S3) form, in a manner analogous to related behaviours observed in spin-cast BCP films[29]. Another observation for films printed on preferential wetting substrates is that narrow terrace regions form at the edges. This phenomenon (for details see Supplementary Fig. S4) is unique to the three-dimensional confined nature of printed patterns and is consistent with observations of the edges of spin-cast films[30] and randomly deposited BCP droplets[31]. A final consideration arises in relation to the effects of thickness. For example, as the thickness of a printed film of 25-26 K PS-b-PMMA increases from ~30 nm (Fig. 4b) to ~70 nm (Fig. 4d), the edge effects diminish significantly. The effect of annealing can also be clearly observed on printed lines. Here, the width decreases and the thickness at the centre increases with annealing on neutral wetting substrates (Supplementary Fig. S5). Collectively, these results indicate that thickness uniformity improves with increasing MW, thickness and strength of wetting interactions with the substrate.

Quantitative analysis of the results obtained on neutral substrates provides additional insights. Figure 4e illustrates the morphologies

schematically, and defines key geometrical parameters, where t and δh correspond to the average thickness immediately after printing and the increase in thickness at the edge due to annealing, respectively. Figure 4f shows the dependence of δh on t for two different MWs. Consistent with the findings described already, the results indicate that the edge effects diminish with increasing thickness and MW. Furthermore, δh increases with annealing time (Fig. 4g; see Supplementary Fig. S6 for images). An inference is that dewetting of PS-b-PMMA chains on neutral substrates plays a crucial role in determining the final thickness profile. Given the perpendicular orientation of assembled domains with respect to the substrate across the entire printed areas, including the edges (Supplementary Fig. S7), one interpretation is that the PS and PMMA chains locally face the methyl methacrylate and styrene monomers of the random copolymer mat, respectively. As such, both blocks prefer to minimize contact with the substrate. With sufficient mobility (that is, low MW, long annealing times), motion occurs at the edges of the films to increase the local thickness. In spite of these diverse, coupled effects, the data of Fig. 4 indicate that highly uniform films are possible for an optimized selection of thickness and annealing conditions. This capability is critically important for practical applications.

Directed self-assembly of printed BCP films

Most applications also require pattern perfection and precise registration in the architecture of the BCP domains within each printed region. The printing schemes described here are compatible with DSA techniques that make use of both chemically[1,8,9] and topographically[10,32,33] patterned substrates. Figure 5 summarizes examples of the former, where the substrate presents guiding stripes of PS mats (Fig. 5a) spaced by regions functionalized with a random copolymer brush to minimize the interfacial energy of lamellae-forming BCP films with perpendicularly oriented domains registered to the guiding stripes[34]. The periodicity of these stripes (~15 nm wide) is 84 nm, corresponding to two and three times the value of L_0 for the 37-37 K and 25-26 K PS-b-PMMA inks, respectively. Figure 5b,c shows results of defect-free directed assembly of lines of BCP printed onto this type of substrate. One in every two (Fig. 5b, 37-37 K) and three (Fig. 5c, 25-26 K) of the PS domains appears brighter in these images, due to differences in the chemistry[34] of the underlying patterns, as observed directly in the regions without printed BCPs. An AFM image (Fig. 5d) of an isolated line further highlights the self-assembly process, which results in a doubling of the density of the underlying pattern. As a demonstration of DSA with multiple periodicities on the same substrate, Fig. 5e presents an SEM image of printed lines of BCPs with two different MWs. The results demonstrate successful DSA of nanoscale domains with two different periodicities on exactly the same chemical pattern. The DSA of BCP films of discrete sizes is demonstrated in Fig. 5f,g. Representative SEM images show defect-free alignment of the domains with respect to the underlying chemical pattern. The wetting behaviour of BCP films printed on neutral and chemical patterned substrates is different. For example, edge effects after annealing are minimal for thin (~20 nm) printed films of 25-26 K PS-b-PMMA on chemical patterns (Fig. 5h). Such effects are consistent with behaviour lying between those of preferential and neutral substrates. One explanation is that the PS stripes pin the PS domains of the BCP, thereby preventing movement at the edges of the film, similar to the case with preferential wetting.

Finally, we demonstrate the compatibility of printing with DSA based on surface topography, that is, graphoepitaxy (Fig. 6). In this case, the substrate presents topographical (~70 nm deep and ~260 nm wide) features consisting of lines of hydrogen silsesquioxane (~70 nm thick) patterned by electron beam lithography on a neutral substrate (Fig. 6a). The PMMA block preferentially wets the hydrogen silsesquioxane sidewall of the trenches, and the bottoms of the trenches are neutral. Under these boundary conditions[35], the lamellar BCP domains orient perpendicular to the substrate and exhibit a high level of orientational alignment along the axis of the trenches (Fig. 6b,c). The effects of DSA and graphoepitaxy are clearly observable near the sidewalls that face away from the patterned regions. Here, favoured interactions between the PMMA block and the hydrogen silsesquioxane result in movement of BCPs from micrometres away to the central axis of the line (Supplementary Fig. S8). A unique capability is printing lines along the long axis of the trench to selectively fill these areas with BCPs for directed assembly (Fig. 6d). Printing a cylinder-forming BCP allows the generation of guided arrays of dots (Fig. 6e) in selected trenches. The results demonstrate the applicability of the approach to producing a range of complex geometries that may be needed in integrated circuit layouts[15]. Using two BCP inks with different MWs enables the creation of domain structures with two different periodicities within the same trench area, as shown in Fig. 6f,g. Whereas templates for DSA using chemical patterns are optimum when the period of the chemical pattern is an integral multiple of the L_0 of the different-MW BCPs that are printed, templates for DSA using topographic patterns are substantially more forgiving with respect to commensurability constraints and can be used with a wide range of BCPs to create patterns with different periods in a single layer.

Conclusions

In summary, the findings reported here illustrate that direct, additive jet printing and self-assembly of BCPs can be used together to form deterministically defined structures in wide-ranging, hierarchical patterns with length scales from centimetres down to ~10 nm. A critical feature of this scheme, particularly for envisioned applications in advanced nanolithography, is that multiple BCPs with different MWs and compositions, or mixtures of them, can be printed onto a single substrate, thereby providing access to patterns with diverse geometries and feature sizes. We expect that, with modest adjustments, these printing approaches can be applied to other BCP chemistries, morphologies and DSA strategies.

Methods

Preparation of neutral wetting substrates. Silicon wafers (⟨100⟩, WRS Materials) were cleaned in Piranha solution (H_2SO_4:H_2O_2 = 7:3) at 130 °C for 30 min and then rinsed with water for 5 min, three times, then dried with nitrogen. A 0.2 wt% solution (toluene) of crosslinkable random copolymer (57% styrene, 39% methyl methacrylate and 4% glycidyl methacrylate, synthesized as described previously[36]) was spin-cast onto the clean silicon wafers and crosslinked at 250 °C for 5 min in a glove box filled with nitrogen.

Preparation of chemically patterned substrates. The chemical patterns consisted of stripes of a crosslinked PS mat separated by regions functionalized with a random copolymer brush (hydroxyl-terminated, 41% styrene, 59% methyl methacrylate)[34]. Patterns were prepared with 193 nm immersion lithography using an ASML XT:1900Gi scanner as described previously[37].

Preparation of topographically patterned substrates. A 70-nm-thick layer of hydrogen silsesquioxane (Dow Corning) was spin-cast on a crosslinked random copolymer mat and patterned with electron-beam lithography (JEOL JBX-6000FS). The exposed regions of the hydrogen silsesquioxane remain after development to serve as the sidewalls of the trenches.

Nozzle and ink preparation. Pre-pulled glass pipettes (World Precision Instruments) with tip inner diameters of 500 nm, 1, 2, 5 and 10 μm were sputter-coated (Denton, Desk II TSC) with Au/Pd. Metal-coated nozzles were treated with a hydrophobic solution (0.1% perfluorodecanethiol in *N*,*N*-dimethylformamide) before printing for 10 min, and then dipped in *N*,*N*-dimethylformamide for 10 s and dried with air. A dilute (for example, 0.1%) solution of PS-b-PMMA (25-26, 37-37 and 46-21 kg mol^{-1}, Polymer Source) in 1,2,4-trichlorobenzene (≥99%, Sigma Aldrich), passed through a syringe filter (PTFE membrane, Acrodisk) with a pore size of 0.2 μm, served as the ink.

Electrohydrodynamic jet printing and thermal annealing of BCP films. A voltage (300–450 V) was applied between a metal-coated glass capillary and a grounded substrate with a standoff height of ~30 μm. Spatial control of the printing

process was provided by a five-axis stage interfaced to a computer that allowed coordinated control of the voltage applied to the nozzle[38]. Unless otherwise stated, printed BCP films were annealed at 220 °C for 5 min in a glove box filled with nitrogen.

Characterization of printed BCP films. The surface morphologies of the printed BCP films were imaged with a field-emission SEM (Hitachi S-4800) at 1 kV. The topography of the films was analysed with an AFM (Asylum Research MFP-3D) in tapping mode using a silicon tip with aluminium reflex coating (Budget Sensors).

Received 14 March 2013; accepted 16 July 2013; published online 25 August 2013

References

1. Ruiz, R. *et al.* Density multiplication and improved lithography by directed block copolymer assembly. *Science* **321,** 936–939 (2008).
2. Lopes, W. A. & Jaeger, H. M. Hierarchical self-assembly of metal nanostructures on diblock copolymer scaffolds. *Nature* **414,** 735–738 (2001).
3. Bai, J. W., Zhong, X., Jiang, S., Huang, Y. & Duan, X. F. Graphene nanomesh. *Nature Nanotech.* **5,** 190–194 (2010).
4. Thurn-Albrecht, T. *et al.* Ultrahigh-density nanowire arrays grown in self-assembled diblock copolymer templates. *Science* **290,** 2126–2129 (2000).
5. Bates, F. S. & Fredrickson, G. H. Block copolymer thermodynamics—theory and experiment. *Annu. Rev. Phys. Chem.* **41,** 525–557 (1990).
6. Park, M., Harrison, C., Chaikin, P. M., Register, R. A. & Adamson, D. H. Block copolymer lithography: periodic arrays of similar to 10(11) holes in 1 square centimeter. *Science* **276,** 1401–1404 (1997).
7. Bang, J., Jeong, U., Ryu, D. Y., Russell, T. P. & Hawker, C. J. Block copolymer nanolithography: translation of molecular level control to nanoscale patterns. *Adv. Mater.* **21,** 4769–4792 (2009).
8. Kim, S. O. *et al.* Epitaxial self-assembly of block copolymers on lithographically defined nanopatterned substrates. *Nature* **424,** 411–414 (2003).
9. Cheng, J. Y., Rettner, C. T., Sanders, D. P., Kim, H. C. & Hinsberg, W. D. Dense self-assembly on sparse chemical patterns: rectifying and multiplying lithographic patterns using block copolymers. *Adv. Mater.* **20,** 3155–3158 (2008).
10. Segalman, R. A., Yokoyama, H. & Kramer, E. J. Graphoepitaxy of spherical domain block copolymer films. *Adv. Mater.* **13,** 1152–1155 (2001).
11. Park, S. *et al.* Macroscopic 10-terabit-per-square-inch arrays from block copolymers with lateral order. *Science* **323,** 1030–1033 (2009).
12. Yang, J. K. W. *et al.* Complex self-assembled patterns using sparse commensurate templates with locally varying motifs. *Nature Nanotech.* **5,** 256–260 (2010).
13. Bita, I. *et al.* Graphoepitaxy of self-assembled block copolymers on two-dimensional periodic patterned templates. *Science* **321,** 939–943 (2008).
14. Stoykovich, M. P. *et al.* Directed assembly of block copolymer blends into nonregular device-oriented structures. *Science* **308,** 1442–1446 (2005).
15. Stoykovich, M. P. *et al.* Directed self-assembly of block copolymers for nanolithography: fabrication of isolated features and essential integrated circuit geometries. *ACS Nano* **1,** 168–175 (2007).
16. Bosworth, J. K., Black, C. T. & Ober, C. K. Selective area control of self-assembled pattern architecture using a lithographically patternable block copolymer. *ACS Nano* **3,** 1761–1766 (2009).
17. Son, J. G., Chang, J. B., Berggren, K. K. & Ross, C. A. Assembly of sub-10-nm block copolymer patterns with mixed morphology and period using electron irradiation and solvent annealing. *Nano Lett.* **11,** 5079–5084 (2011).
18. Wan, L. *et al.* Fabrication of templates with rectangular bits on circular tracks by combining block copolymer directed self-assembly and nanoimprint lithography. *J. Micro-Nanolith. Mem.* **11,** 031405 (2012).
19. Park, J. U. *et al.* High-resolution electrohydrodynamic jet printing. *Nature Mater.* **6,** 782–789 (2007).
20. Park, J. U., Lee, J. H., Paik, U., Lu, Y. & Rogers, J. A. Nanoscale patterns of oligonucleotides formed by electrohydrodynamic jet printing with applications in biosensing and nanomaterials assembly. *Nano Lett.* **8,** 4210–4216 (2008).
21. Galliker, P. *et al.* Direct printing of nanostructures by electrostatic autofocussing of ink nanodroplets. *Nature Commun.* **3,** 890 (2012).
22. Sutanto, E. *et al.* A multimaterial electrohydrodynamic jet (E-jet) printing system. *J. Micromech. Microeng.* **22,** 045008 (2012).
23. Ryu, D. Y., Shin, K., Drockenmuller, E., Hawker, C. J. & Russell, T. P. A generalized approach to the modification of solid surfaces. *Science* **308,** 236–239 (2005).
24. Han, E., Stuen, K. O., La, Y. H., Nealey, P. F. & Gopalan, P. Effect of composition of substrate-modifying random copolymers on the orientation of symmetric and asymmetric diblock copolymer domains. *Macromolecules* **41,** 9090–9097 (2008).
25. Kang, H. I., Soltman, D. & Subramanian, V. Hydrostatic optimization of inkjet-printed films. *Langmuir* **26,** 11568–11573 (2010).
26. Sivaniah, E. *et al.* Symmetric diblock copolymer thin films on rough substrates: microdomain periodicity in pure and blended films. *Macromolecules* **41,** 2584–2592 (2008).
27. Hashimoto, T., Yamasaki, K., Koizumi, S. & Hasegawa, H. Ordered structure in blends of block copolymers. 1. Miscibility criterion for lamellar block copolymers. *Macromolecules* **26,** 2895–2904 (1993).
28. Yamaguchi, D., Hasegawa, H. & Hashimoto, T. A phase diagram for the binary blends of nearly symmetric diblock copolymers. 2. Parameter space of temperature and blend composition. *Macromolecules* **34,** 6506–6518 (2001).
29. Peters, R. D., Yang, X. M. & Nealey, P. F. Morphology of thin films of diblock copolymers on surfaces micropatterned with regions of different interfacial energy. *Macromolecules* **35,** 1822–1834 (2002).
30. Green, P. F. & Limary, R. Block copolymer thin films: pattern formation and phase behavior. *Adv. Colloid Interface Sci.* **94,** 53–81 (2001).
31. Croll, A. B., Massa, M. V., Matsen, M. W. & Dalnoki-Veress, K. Droplet shape of an anisotropic liquid. *Phys. Rev. Lett.* **97,** 204502 (2006).
32. Chai, J., Wang, D., Fan, X. N. & Buriak, J. M. Assembly of aligned linear metallic patterns on silicon. *Nature Nanotech.* **2,** 500–506 (2007).
33. Cheng, J. Y., Mayes, A. M. & Ross, C. A. Nanostructure engineering by templated self-assembly of block copolymers. *Nature Mater.* **3,** 823–828 (2004).
34. Liu, C. C. *et al.* Fabrication of lithographically defined chemically patterned polymer brushes and mats. *Macromolecules* **44,** 1876–1885 (2011).
35. Park, S. M. *et al.* Directed assembly of lamellae-forming block copolymers by using chemically and topographically patterned substrates. *Adv. Mater.* **19,** 607–611 (2007).
36. Han, E. & Gopalan, P. Cross-linked random copolymer mats as ultrathin nonpreferential layers for block copolymer self-assembly. *Langmuir* **26,** 1311–1315 (2010).
37. Delgadillo, P. A. R. *et al.* Implementation of a chemo-epitaxy flow for directed self-assembly on 300-mm wafer processing equipment. *J. Micro-Nanolith. Mem.* **11,** 031302 (2012).
38. Shigeta, K. *et al.* Functional protein microarrays by electrohydrodynamic jet printing. *Anal. Chem.* **84,** 10012–10018 (2012).

Acknowledgements

This work was supported by the Center for Nanoscale Chemical Electrical Mechanical Manufacturing Systems at the University of Illinois (funded by the National Science Foundation under grant CMMI-0749028). The authors acknowledge R. Gronheid and P. Rincon Delgadillo for providing the chemically patterned substrates. C.S. and H.A. were partially supported by the Basic Science Research Program through the National Research Foundation of Korea funded by the Ministry of Education, Science and Technology (2012R1A6A1029029). The authors thank S. Maclaren and K. Chow for support with AFM and electron-beam lithography, respectively. AFM and SEM studies were carried out in the Frederick Seitz Materials Research Laboratory Central Facilities, University of Illinois.

Author contributions

M.S.O. conceived the idea, designed the experiments and analysed the data. M.S.O and C.S. performed the experiments. L.W. prepared the neutral and chemically patterned substrates. E.S., P.M.F. and A.G.A. contributed to the printing systems. P.F.N., H.A. and J.A.R. provided technical guidance. M.S.O. and J.A.R. co-wrote the paper. All authors discussed the results and commented on the manuscript.

Additional information

Supplementary information is available in the online version of the paper. Reprints and permissions information is available online at www.nature.com/reprints. Correspondence and requests for materials should be addressed to J.A.R. and H.A.

Competing financial interests

The authors declare no competing financial interests.

nature nanotechnology

SUPPLEMENTARY INFORMATION

DOI: 10.1038/NNANO.2013.160

Hierarchical Patterns of Three Dimensional Block-Copolymer Films Formed by Electrohydrodynamic Jet Printing and Self-Assembly

Supplementary Information

M. Serdar Onses*, Chiho Song*, Lance Williamson, Erick Sutanto, Placid M. Ferreira, Andrew G. Alleyne, Paul F. Nealey, Heejoon Ahn, John A. Rogers

To whom correspondence should be addressed:

E-mail: jrogers@illinois.edu, ahn@hanyang.ac.kr

* *These authors contributed equally to this work.*

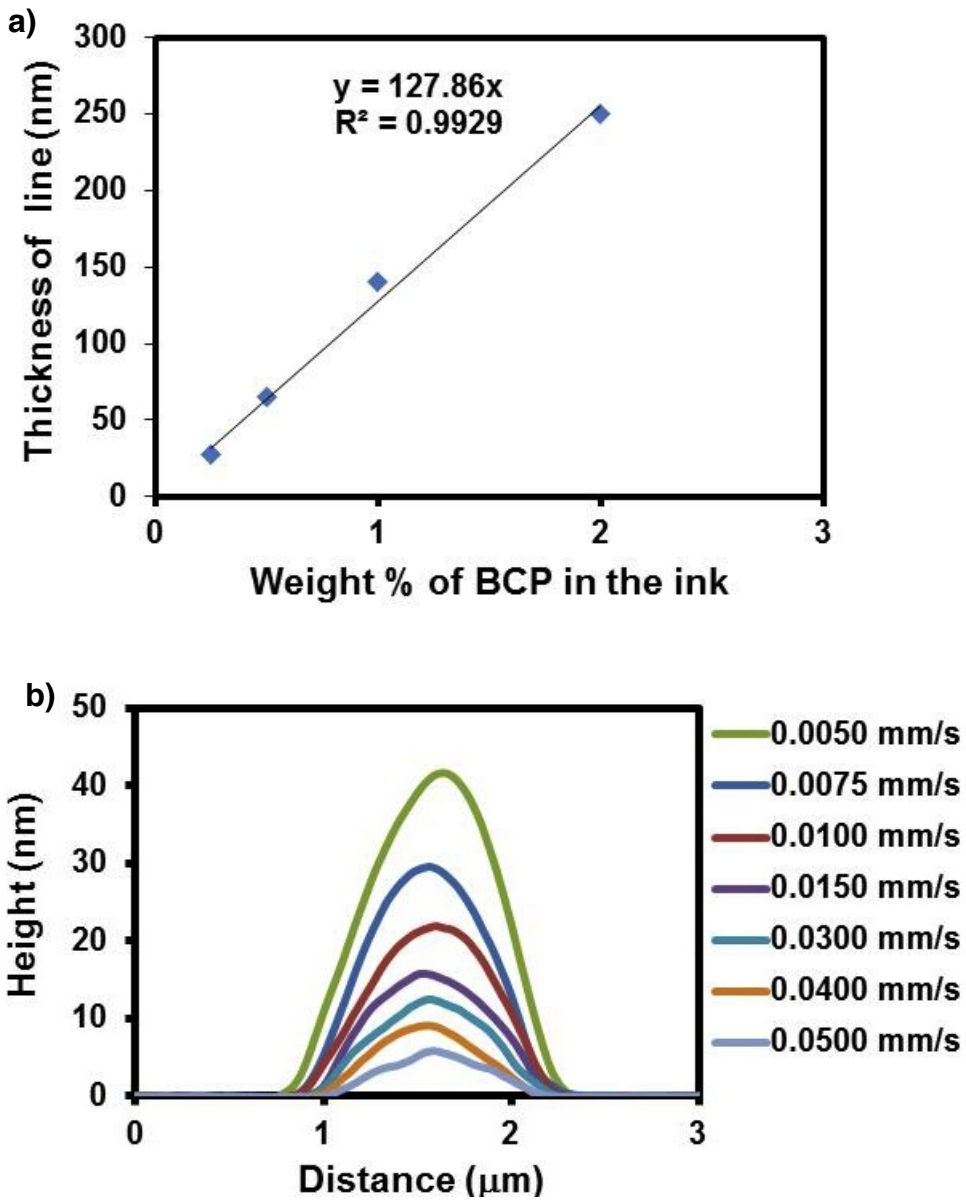

Figure S1. Effect of the weight % of BCP in the ink and printing speed on the thickness of printed lines. a) Thickness of printed lines as a function of the weight % of PS-*b*-PMMA in the ink. The data points in the plot correspond to the average thickness of the ~3 μm lines printed with a 5 μm internal diameter nozzle. b) The height profiles of printed lines as a function of printing speed. The printing was performed using a 1 μm internal diameter nozzle.

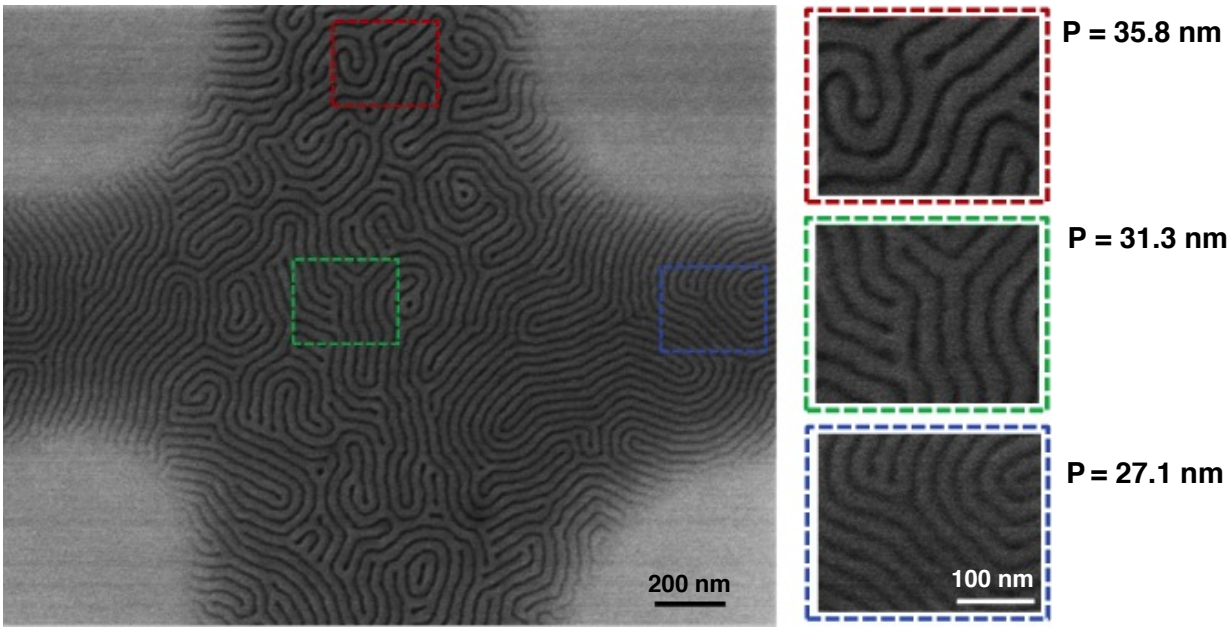

Figure S2. Mixing of printed BCPs on the surface. SEM image shows the morphology of two crossing lines of different molecular weight BCPs. First a linear pattern of 37-37 K (vertical direction) and then 25-26 K (horizontal direction) PS-*b*-PMMA was printed. Thermal annealing was performed at 220 °C for 5 min.

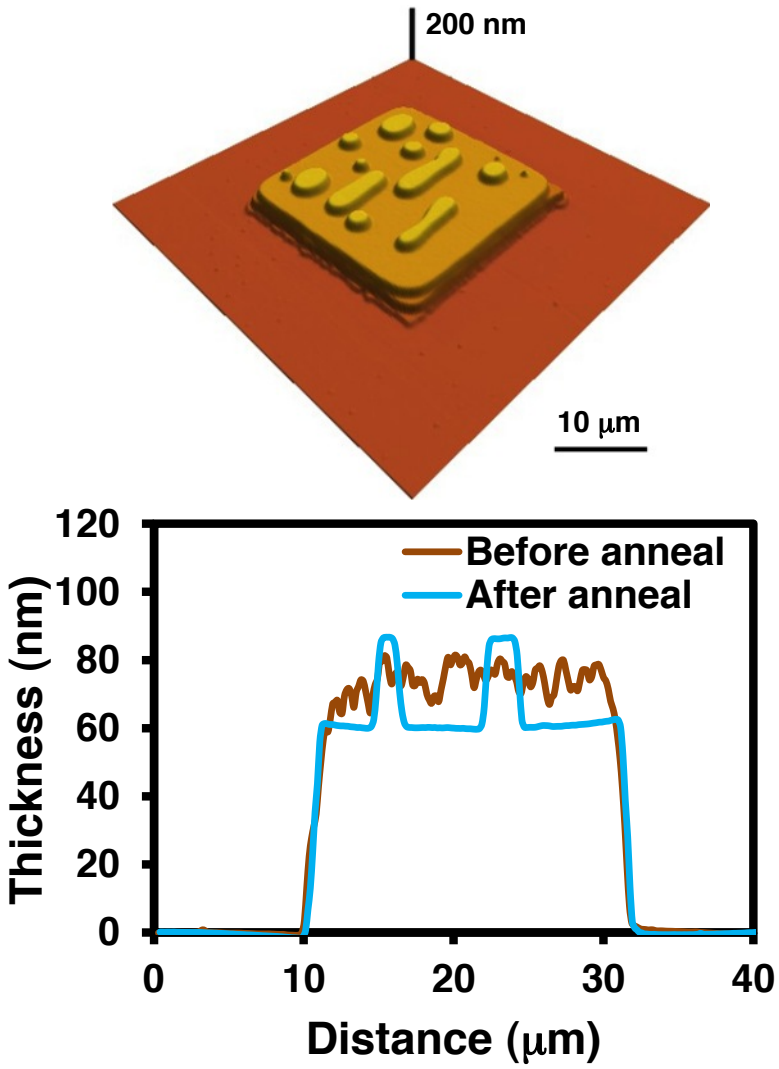

Figure S3. Island/hole formation in printed BCP films. AFM image (after annealing) and cross-sectional height profile of printed 25-26 K PS-*b*-PMMA on a preferential wetting substrate.

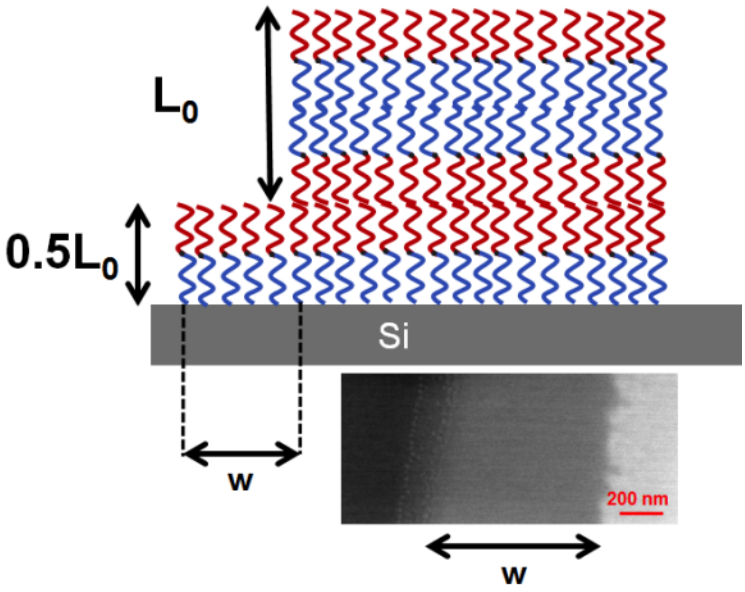

Figure S4. Schematic of the terrace formation on preferential wetting substrates. The schematic is based on the height profile given in Figure 4c of the manuscript and the previously proposed mechanism for a BCP droplet.[1]

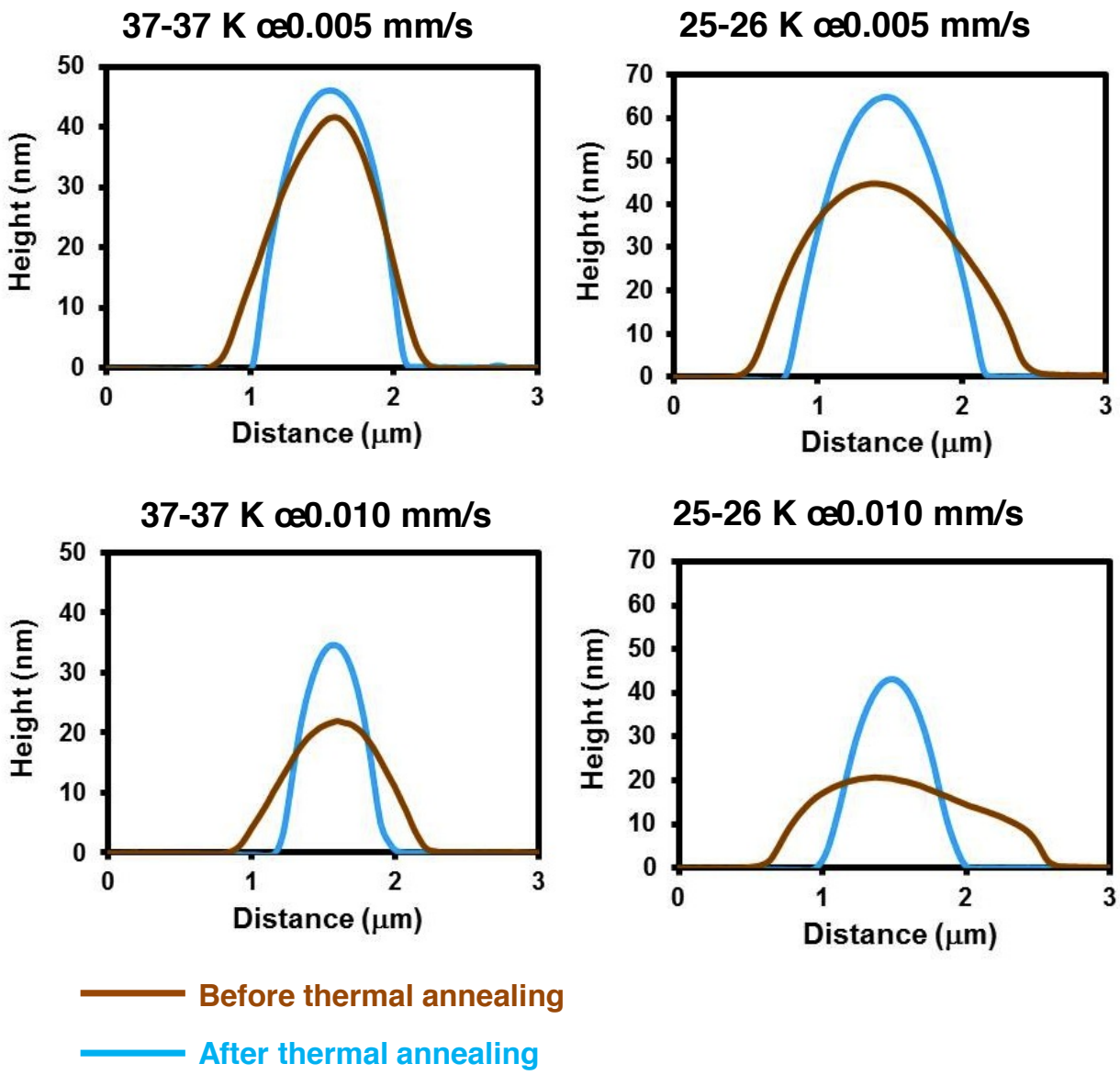

Figure S5. The effect of thermal annealing on the cross-sectional height profiles of individual printed BCP lines. The molecular weight of PS-*b*-PMMA and printing speed are given at the top of the plots. The substrate is neutral wetting for the all cases.

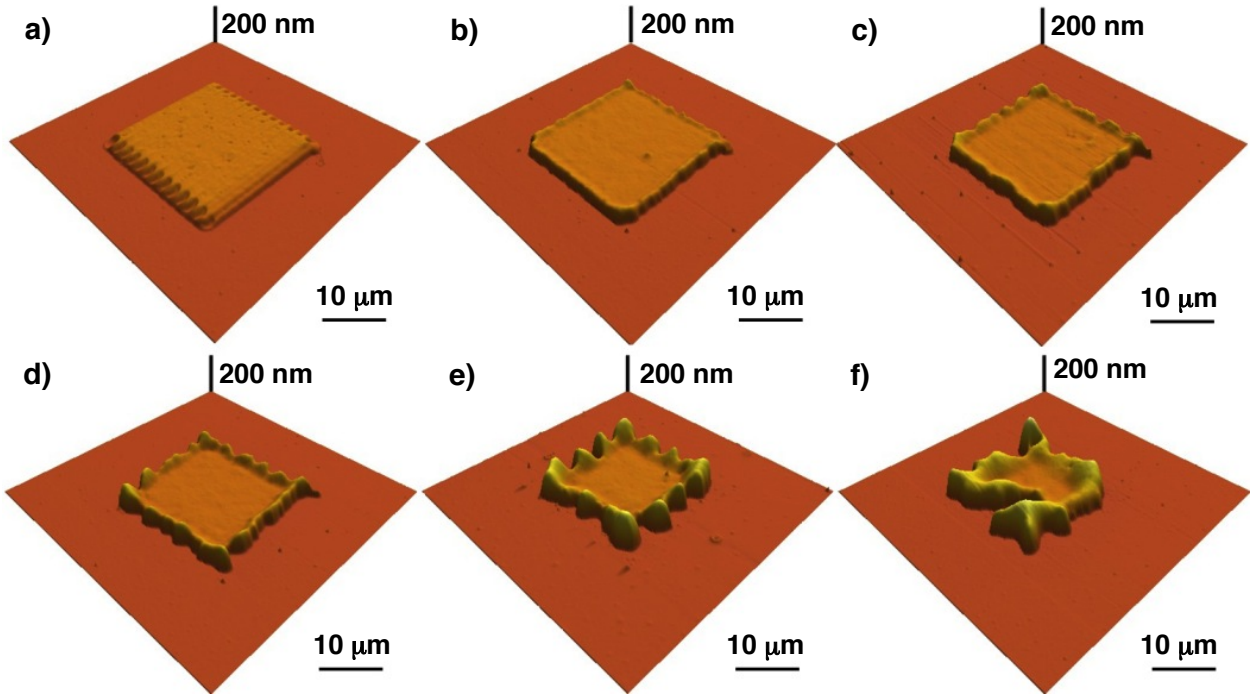

Figure S6. Effect of the annealing time on the height profile of printed BCP films. AFM image of 20 μm wide square films of 25-26 K PS-*b*-PMMA printed on a neutral wetting substrate. a) Before annealing, b-e) After annealing at 220 ^{o}C for b) 2 min, c) 5 min, d) 15 min, e) 1 h and f) 5h.

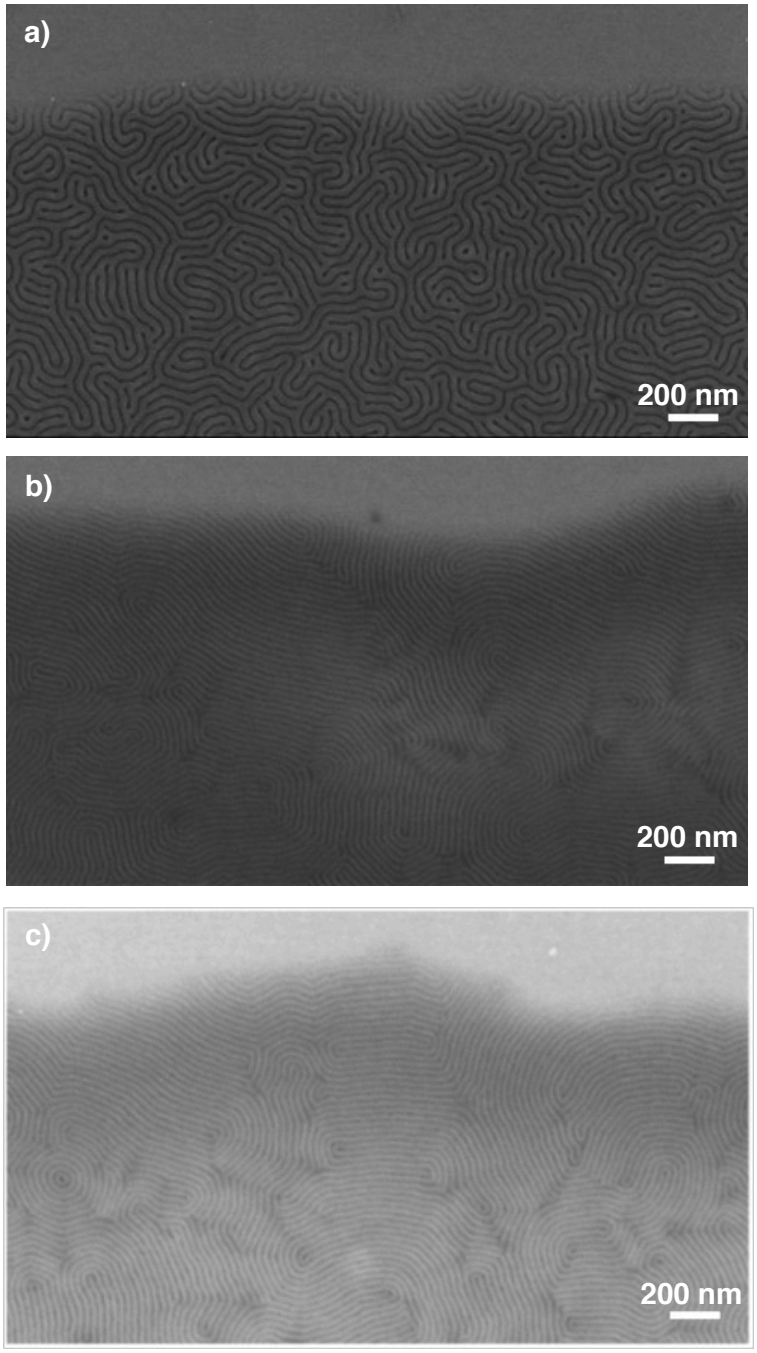

Figure S7. BCP films near the edge of a printed square. SEM images were taken at the edges of the films presented in Figure 4 of the manuscript. a) ~30 nm film of 37-37 K (Fig 4a), b) ~30 nm film of 25-26 K (Fig 4b), c) ~70 nm film of 25-26 K (Fig 4d) PS-*b*-PMMA. The substrate is neutral wetting for the all cases.

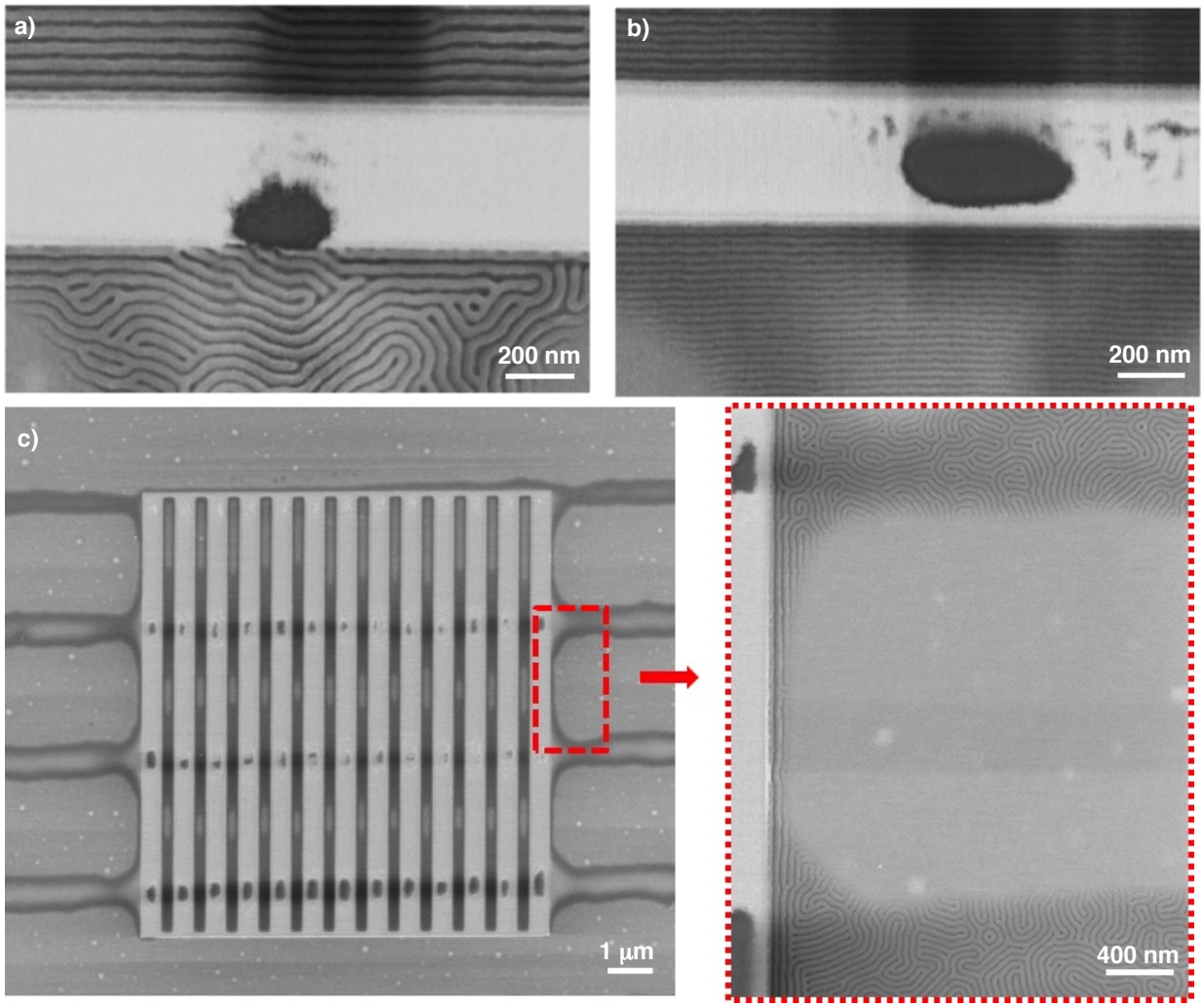

Figure S8. Printed BCP lines near the wall. SEM images of individual printed lines near the edge of the topographical patterns, for MWs of (a) 37-37 K and (b) 25-26 K. c) Movement of 37-37 K PS-*b*-PMMA microns away from to the central axis of the line near the wall. The wall is 70 nm high and preferential wetting to the PMMA block. The bottom substrate is neutral wetting.

References

1. Croll, A. B., Massa, M. V., Matsen, M. W. & Dalnoki-Veress, K. Droplet shape of an anisotropic liquid. *Phys. Rev. Lett.* **97**, 204502 (2006).